

THE ORIGINS OF APERIODICITIES IN SENSORY NEURON ENTRAINMENT

H. L. READ and R. M. SIEGEL*

Center for Molecular and Behavioral Neuroscience, Rutgers University, 197 University Avenue,
Newark, NJ 07102, U.S.A.

Abstract—Aperiodic entrainment to rhythmic sensory input was obtained with either a single neuron or an excitatory network model, without addition of a stochastic or “noisy” element. The entrainment properties of primary sensory neurons were well captured by the dynamics of the Hodgkin–Huxley ordinary differential equations with a quiescent resting state or threshold for spike output. The frequency–amplitude parameter space was compressed and aperiodic regimes were small in comparison to those of periodically activated pacemaker-like neurons. Transitions between phase-locked and aperiodic entrainment patterns were predictable and determined by the equation dynamics, supporting the contention that some aperiodicities observed *in situ* arise from the inherent membrane properties of neurons. When the rhythmically activated neuron was embedded in an excitatory network of Hodgkin–Huxley neurons with heterogeneous synaptic delays, aperiodic entrainment patterns were more frequently encountered and these were associated with asynchronous output from the network. Embedding the rhythmically activated neuron in a network with synaptic delays greatly reduced the range of entrained spike frequencies and increased the variability in the neuronal firing.

The temporal coding of sensory stimuli may be dependent on these findings. Sensory stimuli are signaled in the periphery by a mixture of periodic and irregular interspike intervals. Most models of such temporal codes assume intrinsic rhythmicity arising from the ionic currents, with variations attributed to membrane or synaptic noise. In contrast, we demonstrate irregular neural codes that arise completely in the absence of noise. In the proposed model, the sources of these irregular sensory patterns are the extensive cross-connections and resultant interactions between neurons.

The balance between the regular and irregular entrainment of a neuron *in situ* could uniquely identify a stimulus. Other biological mechanisms of modifying the entrainment properties and promoting aperiodic entrainment are discussed. Copyright © 1996 IBRO. Published by Elsevier Science Ltd.

Key words: sensory neuron, asynchronous, dynamic, entrainment, chaos.

One of the basic organizing principles of coherent activity in the mammalian nervous system is the genesis of rhythms. Neurons are capable of generating cyclic repetitive output, the inherent frequency of which depends on the complement of membrane conductances underlying its spiking behavior. If a neuron is driven with a sufficiently large amplitude rhythmic membrane depolarization, it will generate action potentials (spikes) that occur at a fixed time in relation to the stimulus for a limited range of stimulus frequencies. For example, somatosensory fibers can spike with a fixed time delay following the onset of each cycle of membrane depolarization that occurs with rhythmic mechanical vibration of the skin.⁴⁵ Spiking is considered “phase-locked” or “periodically entrained” to the stimulus when there is a fixed temporal relation between the cycle (or phase) of input and the cycle of output (spiking) of a neuron. If the stimulus amplitude is sufficiently large, a somato-

sensory fiber will generate one spike for every stimulus cycle, yielding a periodic entrainment pattern of 1:1 (cycles of input : spike output).

Simple 1:1 entrainment patterns are rare in the mammalian CNS, the more common observation being a spike pattern that is “phase related” to the period of rhythmic input, but not periodic itself. Physiologists generally attribute such “jitter” or aperiodic entrainment to ion channel and synaptic noise; however, a source of this irregularity that is often overlooked is that arising from the entrainment process of the neural system itself.

Previous physiological and theoretical studies have focused on the entrainment properties of pacemaker-like neurons that spontaneously oscillate at rest.^{1,8,17,19,21,27,32,38,39} In these biological models, a resting oscillatory state was created by lowering the external calcium concentrations^{1,27} or by injecting depolarizing bias current.^{8,17,19,21} In either case, periodic input was able to generate aperiodic spike trains in the driven neuron. Though these model systems were simple, they were biological and there was some debate as to the origin of aperiodic entrainment patterns.^{19,21} These

*To whom correspondence should be addressed.

Abbreviations: HH, Hodgkin–Huxley; ISI, interspike interval; nISI, normalized ISI; PSC, postsynaptic current.

Table 1. Notation of variables used

	Values or equations	Units	Variables
C_m	1.0	$\mu\text{F}/\text{cm}^2$	Membrane capacity
Temp.	6.3	$^\circ\text{C}$	Temperature
g_{Na}	120.0	mS/cm^2	Sodium conductance
g_{K}	36.0	mS/cm^2	Potassium conductance
g_{L}	0.1	mS/cm^2	Leak conductance
I_{input}	$I_{\text{cos}(t)} + I_{\text{syn}(t)}$	$\mu\text{A}/\text{cm}^2$	Input current
$I_{\text{cos}(t)}$	$A\cos(\omega t)$	$\mu\text{A}/\text{cm}^2$	Oscillatory input current
ω	[0–1]	ms^{-1}	Angular frequency
f	$\omega/2\pi$	ms^{-1}	Frequency
T	$1/f$	ms	Period for oscillatory input
A	[0–100]	$\mu\text{A}/\text{cm}^2$	Input current amplitude
$I_{\text{syn}(t)}$	see		Synaptic input
S_{ij}	0.142	mS/cm^2	Synaptic strength

aperiodic entrainment states exist in simplified mathematical models which do not incorporate noise.^{1,17,18,19,21,27,31,32} Furthermore, these aperiodic entrainment patterns were obtained in a parametric and predictable manner similar to that of periodic entrainment. These findings supported the contention that aperiodicities in biological systems are, in part, a product of the entrainment process.

While the spontaneous oscillatory state is a natural one for cardiac fibers and for pacemaker-like neurons, it is not the natural resting state for a broad spectrum of neurons in the mammalian peripheral and central nervous systems.^{11,33,40,45} A variety of sensory neurons, including cutaneous afferents, gustatory neurons, warm fibers and bulboreticular neurons, have zero or low spontaneous firing rates.^{4,11,33,40,45} The dynamics of such neurons have not been realistically captured with computational studies that assume baseline periodicity prior to entrainment. Furthermore, these studies assumed and required the acquisition of continuous intracellular membrane potential data, a technical feat rarely achieved in the natural state of the neuron (i.e. in awake behaving animals).

The present study seeks to explore in detail the entrainment properties of neurons that are silent prior to sensory or afferent input. Although there is an examination of intracellular membrane potential, most of the study is aimed at an easily obtained physiological measure, in particular the interspike interval (ISI), to facilitate comparison with experimental data. Sinusoid current is used to drive otherwise quiescent Hodgkin-Huxley (HH)-type model neurons. In addition, the aperiodic entrainment patterns of a sinusoid driven HH neuron embedded in a population of synaptically coupled HH neurons are examined, again to more closely approximate *in situ* conditions. The synaptic feedback and delays associated with the population of coupled HH neurons serve to dramatically alter the entrainment properties.

EXPERIMENTAL PROCEDURES

The HH differential equations were used to model the sodium (g_{Na}), potassium (g_{K}) and leak (g_{L}) conductances underlying the action potential.²⁰ These equations were originally developed to model squid axonal current and they were employed here to provide a simple model of sensory neuron action potentials. The differential equations for the active membrane state variables and activation/inactivation rate functions were as follows:

$$C_m dV dt = I_{\text{input}} - g_{\text{Na}} m^3 h (V - V_{\text{Na}}) - g_{\text{K}} n^4 (V - V_{\text{K}}) - g_{\text{L}} (V - V_{\text{L}})$$

$$\frac{dm}{dt} = a_m (1 - m(t)) - \beta_m m(t)$$

$$\frac{dh}{dt} = a_h (1 - h(t)) - \beta_h h(t)$$

$$\frac{dn}{dt} = a_n (1 - n(t)) - \beta_n n(t)$$

$$a_n = 0.1 \frac{\left(\frac{V+10}{10}\right)}{\exp\left(\frac{V+10}{10}\right) - 1}, \beta_n = 0.125 \exp\left(\frac{V}{80}\right)$$

$$a_m = \frac{2.5 \left(\frac{V+25}{25}\right)}{\exp\left(\frac{V+25}{10}\right) - 1}, \beta_m = 4 \exp\left(\frac{V}{18}\right)$$

$$a_h = 0.07 \exp\left(\frac{V}{20}\right), \beta_h = \frac{1}{\exp\left(\frac{V+30}{10}\right) + 1}$$

The variable I_{input} is the input current density (nA/cm^2) and V is the membrane potential difference (mV). The rising rate constants a_m , a_h and a_n account for sodium channel activation, sodium channel inactivation and potassium channel activation, respectively. The decay rate constants for the respective ion channels are β_m , β_h and β_n . The

maximal sodium, potassium and leak conductances are g_{Na} , g_K and g_L (mS/cm²), respectively; the respective ionic reversal potentials are V_{Na} , V_K and V_L . The variable t is time (ms) and C_m is the membrane capacity (μ F/cm²). Temperature, C_m , g_{Na} , g_K and g_L are 6.3°C, 1.0 μ F/cm², 120, 36 and 0.1 μ S/cm², respectively (see Table 1 for appropriate values and abbreviations).

Single model or ‘‘HH’’ neurons are given by a complete set of the equations for a unit area of membrane as outlined above. The computational simplicity of these model neurons allows for extensive parameter mapping of spike entrainment. The Runge–Kutta fourth order numerical integration routine (time step of 0.05 ms) is employed to integrate these differential equations.³⁶ Previous studies of these equations have found qualitatively similar results with lower order methods of integration, such as the Euler method.²¹ However, the fourth order Runge–Kutta method for stiff differential equations is more suitable for quantitative analysis as it introduces less numerical error.¹⁹ Computations were carried out on IBM RS/6000 workstations with 32-bit precision.

The population model consists of 25 coupled HH neurons in a one-dimensional array. Each neuron within the 25-cell array is coupled to its five nearest neighbors on each side via a rapid depolarizing membrane current. The synaptic strengths and delays are the same for all neurons. A Heavyside function was used to model the summed synaptic input current for computational simplicity. The summed synaptic input current to a neuron is modeled according to the following function:

$$I_{syni}(t) = \sum_{j=1}^{n_{syn}} S_{ij} (V_j(t - \tau_{ij}) - V_{th}) H(V_j(t - \tau_{ij}) - V_{th}).$$

$H(x)$ is the Heavyside function (i.e., $H(x) = 0$ for $x \leq 0$; $H(x) = 1$ for $x > 0$). A synaptic potential occurs when $V(t) - V_{th} > 0$. The time course of the model synaptic potential resembles that of biological postsynaptic currents (PSCs). Our model PSCs could be quantitatively described by an a function ($a(t) = t \exp(-t/\sigma)^{2.1a}$ with a time constant, σ , between 0.7 and 1.2 ms, like for example, the hippocampal mossy fiber PSCs.⁵ The maximal synaptic potential amplitude increases in proportion to the level of V_{th} , which was fixed at 50 mV. The synaptic strength constant, S_{ij} , is fixed at 0.142 μ S/cm², which yields a subthreshold synaptic potential in the present model. Thus, a certain degree of synaptic convergence must occur to bring the membrane potential to threshold (see Fig. 6). The conduction delay is the time (τ_{ij}) required for the action potential to travel from the i th to the j th neuron and includes the axonal propagation delay and synaptic delay. The conduction delay between adjacent neurons was fixed at 3 ms. This delay increased linearly with displacement, so that the largest delay was 15 ms for input displaced by five neurons from the source. The number of synaptic inputs to a given neuron (n_{syn}) varied from five to 10 depending on the cell position. Thus, neurons displaced six or less neurons from the borders had $n_{syn} = n_{dis} - 1 + 5$, where n_{dis} is the displacement from the border; all other neurons received 10 synaptic inputs. Neurons were never connected to themselves via recurrent connections. The parameters S_{ij} , τ_{ij} and n_{syn} were based on extensive neuronal simulation to provide a population of single quiescent neurons that would spontaneously oscillate (Siegel and Read, unpublished observation).

The driving current or I_{input} for single and population neurons differed in the following manner. In the single-neuron model, the applied stimulus current was varied according to a cosine function:

$$I_{input} = I_{cos}(t) + I_{syn}(t) I_{cos} = A \cos(\omega t),$$

where $f = \omega/2\pi$. Thus, for the single neuron model I_{syn} was zero and I_{input} was equal to I_{cos} . In the population model, only the central neuron was driven by a sinusoidal current

and population synaptic input; hence, I_{input} is equal to the sum of I_{cos} and I_{syn} for neuron 13. For all neurons except the central neuron in the population model, the input current was synaptic (i.e., $I_{input} = I_{syn}$). The amplitude, A (nA/cm²), and ω (rad/ms) were varied systematically in order to map the amplitude–frequency parameter space. The ISIs were computed as the time between the crossings of 50 mV on the upstroke of the action potential. For all figures, the ISIs have been normalized (nISI) to the driving period ($T = 1/f$), yielding a dimensionless quantity (i.e. nISI = ISI (ms)/ T (ms)). Normalization of the ISIs allowed for comparison of ISIs generated with different sinusoid frequencies.

RESULTS

The sinusoidally driven single neuron: periodic patterns

The single neuron entrainment to the period of sinusoid input current was analysed for a large range of sinusoid amplitudes and periods. Single neuron activity was simulated for 50 s in order to ensure that the initial transients in activity were gone and the output pattern had stabilized. The spike patterns that occurred in the final 10 s of a 50-s simulation were examined for periodicity. Spiking patterns were considered phase-locked if the action potential occurred at a regular phase of the stimulus cycle. The means and standard deviations for nISIs occurring in the 10-s steady-state period were calculated as numerical measures of entrainment.

Spiking of the single HH neuron was temporally locked to the period of sinusoidal current for most stimulus parameters employed; phase-locked patterns varied as a function of stimulus parameters. With low stimulus intensities, frequent but periodic spike failures occurred and resulted in ‘‘higher order’’ entrainment ratios. A common higher order entrainment pattern consisted of three cycles of sinusoid current per spike or a 3:1 ratio (Fig. 1A). (Throughout this paper the terminology $m : n$ refers to m cycles of sinusoid input to n action potentials.) In Fig. 1A, B and D, the sinusoid stimulus was plotted (-15 mV offset) along with the neuron membrane potential to allow for visual comparison of the stimulus phase and spiking pattern. Patterns of 4:1, 5:1, 6:1, 8:1, 9:1, 10:1 and 11:1 were observed as well (e.g., the 11:1 pattern is shown in Fig. 4A); however, these were not as common as the 3:1 pattern of spiking illustrated in Fig. 1A. There was no deviation from a 3:1 phase-locking pattern in the range of stimulus amplitudes including 1500–1515 nA/cm², with a fixed sinusoid period of 19.04 ms ($\omega = 0.31$ ms⁻¹). In the region labeled ‘‘3:1’’ in Fig. 1C, the mean nISI per stimulus condition was 3.0 and the standard deviation was zero, reflecting the stability of 3:1 phase-locking.

Abrupt transitions from stable higher order to stable lower order phase-locking patterns took place when the sinusoid amplitude was increased. For example, when the stimulus amplitude was increased from 1515 to 1520 nA/cm², there was an associated transition from 3:1 to 2:1 phase-locking (e.g., Fig. 1C, $\omega = 0.33$ ms⁻¹). Between the regions of 3:1 and

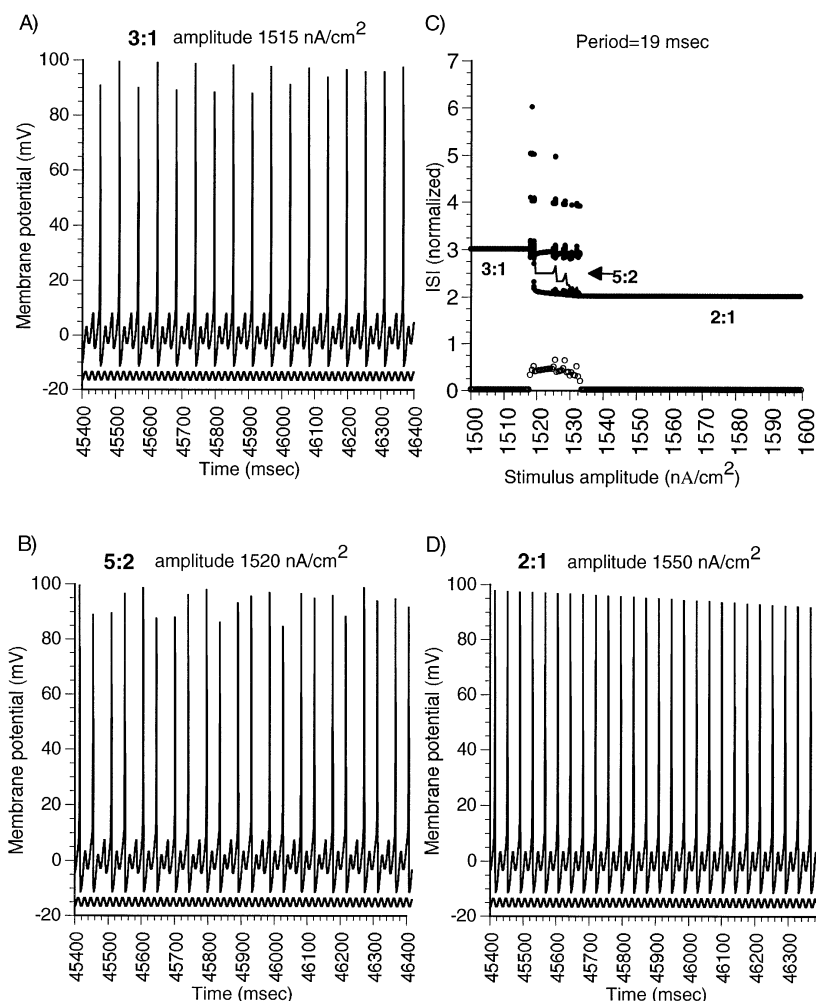


Fig. 1. Entrainment patterns vary systematically with changes in sinusoid amplitude for a fixed period of 19 ms ($\omega = 0.33 \text{ ms}^{-1}$). (A, B, D) Plots of membrane and stimulus potentials during the steady-state period. Phase-locked patterns of 3:1, 5:2 and 2:1 (stimulus cycles : spikes) are elicited with stimulus amplitudes of 1515, 1520 and 1550 nA/cm², as illustrated in A, B and D, respectively. In this and all subsequent voltage plots, the sinusoid potential is offset by -15 mV to allow visual comparison of stimulus and spike phase. Spike amplitudes vary due to aliasing in the graphical output. (C) Normalized ISIs (nISIs; solid circles). The mean nISI (solid line) and the standard deviation (open circles) for the 10-s steady-state period are plotted for a range of stimulus amplitudes. The sinusoid amplitude was varied from 1500 to 1600 nA/cm² in 0.5-nA steps. Note that the regions of 2:1 and 3:1 phase-locking are dominant. The smaller region of 5:2 phase-locking is interleaved between the 2:1 and 3:1 regions; 5:2 phase-locking is associated with a mean nISI of 3.5, as indicated with an arrow. In all plots of amplitude versus nISI, the symbols (open and closed circles) for both nISI and standard deviations form a thick solid line when the values are the same for several amplitudes; standard deviations (open circles) are always of lower value than the nISI (closed circles) or mean nISI (thin line).

2:1 phase-locking, there was an abrupt increase in the nISI standard deviation. Several small regions of stable phase-locking were found inside this border region. For example, the most stable pattern in the "border region" shown in Fig. 1C was the 5:2 pattern (see voltage plot of Fig. 1B). ISI durations of exactly two and three times the stimulus period were interleaved in the 5:2 pattern. Accordingly, the mean nISI (plotted as a line in Fig. 1C, arrow) was 2.5 for the 5:2 pattern. A small nISI standard deviation (0.5) was observed with the 5:2 pattern, reflecting the stable alternating sequence of ISIs. Thus, the 5:2 pattern

was a merging of the stable patterns in the bordering regions of 3:1 and 2:1 phase-locking (Fig. 1). Similarly, an intermediate pattern of 3:2 was found between 2:1 and 1:1 phase-locking regions of the parameter space. The 3:2 was composed of alternating ISIs of two and one times the sinusoid period and a mean nISI of 1.5. Thus, the intermediate 3:2 pattern was a merging of stable patterns, as was the case for 5:2 patterns. The general trend was for fewer spike failures to occur with higher amplitude stimuli.

The order of transitions between entrainment patterns was conserved for different stimulus periods.

For example, the sequence of 3:1, 5:2 and 2:1 patterns elicited with an increase in stimulus amplitude was the same for stimulus periods of 29.9, 20.94 and 19.04 ms. However, the range of stimulus amplitudes eliciting a given pattern varied with stimulus period. Thus, the range of stimulus amplitudes eliciting mean nISIs of 3, 2.5 and 2 (phase-locking of 3:1, 5:2 and 2:1, respectively) was smaller with a stimulus period of 29.9 ms (Fig. 4C) as opposed to 19.04 ms (Fig. 1C).

The order of patterns observed with different stimulus conditions was predictable according to a simple additive rule. For example, entrainment ratios of 3:1 and 2:1 add to generate a ratio of 5:2. Additivity of neighboring phase-locking patterns was a general property of the sinusoid driven HH neuron. This additive property follows the general rule that regions of $(m_1 + m_2) : (n_1 + n_2)$ occur between neighboring patterns of $m_1 : n_1$ and $m_2 : n_2$ (cycles of input : spikes). Phase-locking ratios including 7:2, 8:2, 8:7, 10:9 and 9:8 were observed sandwiched between appropriate neighbors (e.g., 7:2, Fig. 4C). This addition rule is not fortuitous; it is described by the ‘‘Farey sum’’ in number theory and can be demonstrated analytically to describe the parametric sequencing of temporal patterns in certain mathematical and physical oscillating systems.^{10,12,32,39,43} The sequences of summation patterns are called ‘‘Farey sequences’’.

The rigid order of transitions between phase-locking patterns was conserved throughout the frequency–amplitude parameter space. A high resolution map of the mean nISIs for a large range of parameters was generated to illustrate interactions between the amplitude and frequency of sinusoidal stimuli. Stimulus frequency or ω ($2\pi f$) was varied from 0 to 1 ms^{-1} in steps of 0.005 ms^{-1} . Stimulus amplitude was varied from 2 to 80 in steps of $1 \mu\text{A}/\text{cm}^2$. The steps in amplitude used to map large portions of the parameter space (mA/cm^2 ; Fig. 2A) were 2000 times greater than those used to examine Farey sequences in detail ($0.5 \text{ nA}/\text{cm}^2$; Fig. 1, Fig. 3, Fig. 4). Mean nISIs were assigned to a repeating rainbow color spectrum with mean nISIs of 1, 2 and 3 labeled with fuchsia, yellow and green. The exact values of the color spectrum are labeled on the color bar above the graph in Fig. 2A. As known for other excitable or threshold systems, the different phase-locking regions all converged towards a common low-amplitude/frequency limit (Fig. 2A, lower left). The most ‘‘stable’’ or commonly encountered phase-locking pattern was that of 1:1, labeled with a fuchsia red color in Fig. 2A. Such low-frequency firing patterns have also been reported for a broad range of current amplitudes when the driving stimulus was a sustained depolarization²¹ (e.g., motoneurons). The Farey sequences for phase-locking patterns described above were conserved across the entire parameter space. The most prominent summation was that of 2:1 (yellow) and 1:1 (fuchsia red), which yielded a

region of 3:2 (persimmon orange). Smaller stable regions were observed interleaved between the larger regions. For example, the thin green region interleaved between the 3:2 and 1:1 regions corresponds to a 4:3 (mean nISI of 1.25; see color band). Another example of additivity is the thin blue 5:3 region between the 3:2 and 2:1 phase-locking regions. Higher order phase-locking patterns, such as 11:1, 8:1, 6:1 and 4:1, were observed with the lower amplitude and frequency sinusoid driving. The latter regions are labeled in lavender (mean ISIs 4.5) in the parameter map of Fig. 2A. Higher order phase-locking patterns (e.g., see the lavender region) covered relatively less of the parameter space than their lower order counterparts (e.g., 1:1), as has been observed for analogous patterns generated by iterating simple (e.g., unimodal maps) mathematical functions.^{12,16} Finally, with a low amplitude and low frequency of stimulus, multiple spikes occurred on each stimulus cycle. The latter patterns corresponded to fractional mean nISIs. Stable patterns of 1:2, 1:3, 1:4 and 1:5 with corresponding colors of pink, red, orange and yellow were observed (see Fig. 2A).

Sinusoidally driven single neuron: aperiodic patterns

In the transition zones between stable phase-locking regions, there were regions with aperiodic entrainment patterns. The existence of such aperiodic regimes for the HH differential equations was predicted in a linearized version of these equations,² but the extent and nature of these aperiodicities were not explored in detail. Standard deviations for aperiodic nISI sequences were higher than those associated with periodic sequences, and they ranged from 0.5 to 6. Standard deviations of 0 were mapped in black and those with higher values were mapped on a rainbow color spectrum (Fig. 2B, color bar). Standard deviations greater than or equal to 6 were mapped in red in Fig. 2B and standard deviations greater than or equal to 0.6 were mapped in red in the inset of Fig. 2B.

Two large aperiodic regimes were observed and these covered a stimulus frequency range from 33 to 135 Hz. Initially, a low-resolution frequency–amplitude parameter space was mapped for amplitudes between 2 and $80 \mu\text{A}/\text{cm}^2$ (Fig. 2B). For the low-resolution map, steps in amplitude and ω were $1 \mu\text{A}/\text{cm}^2$ and 0.20 ms^{-1} , respectively. For amplitudes near $2 \mu\text{A}/\text{cm}^2$, a large ‘‘aperiodic’’ or highly variable region was obtained with ω values of $0.70\text{--}0.85 \text{ ms}^{-1}$ or with spike frequencies of 111–135 Hz (Fig. 2B). This region was extended to cover ω values of $0.64\text{--}0.85$ when the stimulus amplitude was below $2 \mu\text{A}/\text{cm}^2$ (Fig. 2B, inset). A second aperiodic region was apparent with the high-resolution map when the stimulus amplitudes were below $2 \mu\text{A}/\text{cm}^2$ (Fig. 2B, inset and arrow). The region between amplitudes of 1.5 and 2.6 was mapped at a higher resolution with steps in amplitude of $0.005 \mu\text{A}/\text{cm}^2$ and ω of 0.20 ms^{-1} . Aperiodic patterns were found for ω

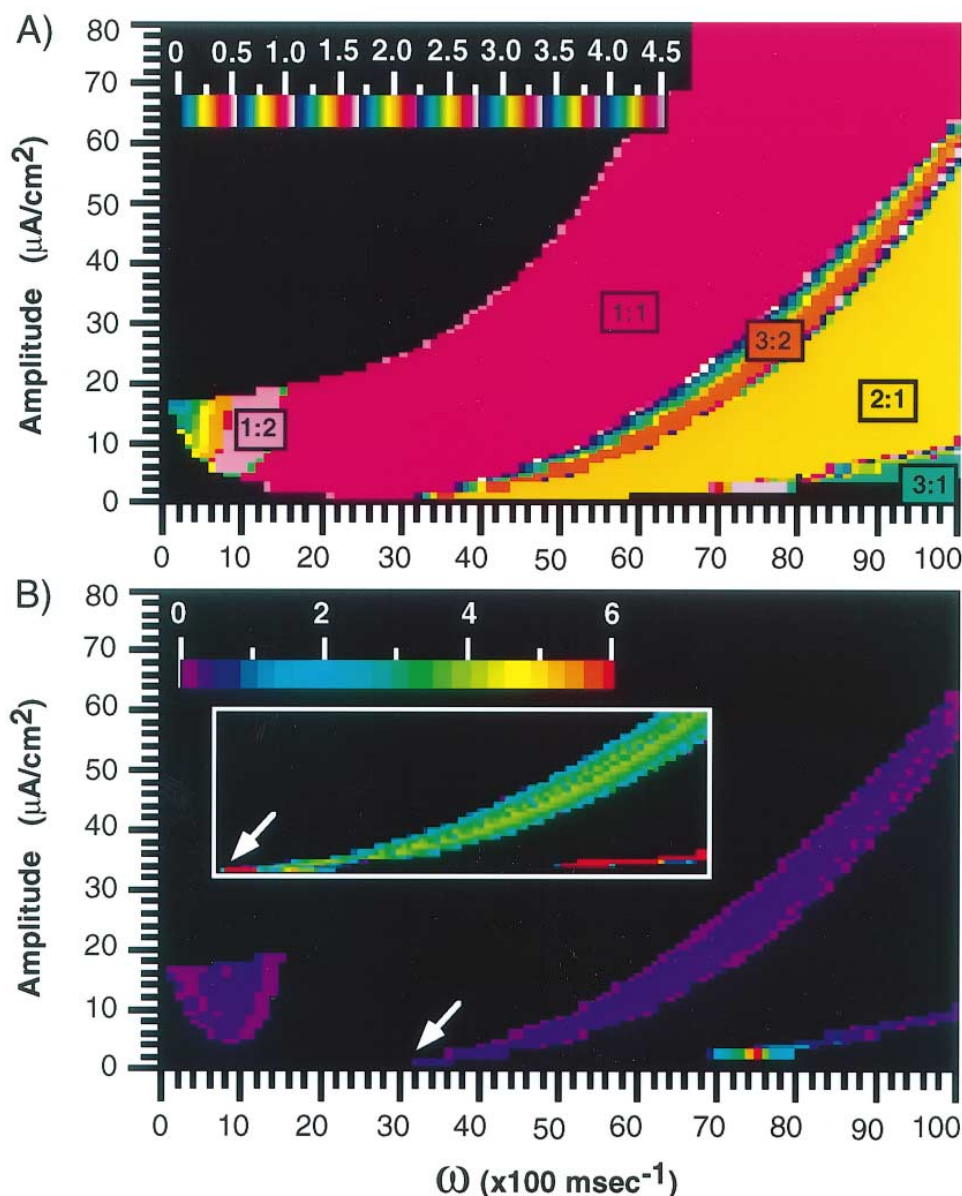


Fig. 2. Frequency–amplitude parameter space. (A) The mean normalized ISIs (nISIs) for a 10-s steady-state period are plotted as a function of the amplitude and ω of sinusoid stimulus (see). Amplitude and ω are incremented in steps of $1 \mu\text{A}/\text{cm}^2$ and 0.005 ms^{-1} , respectively. Mean nISIs are plotted on a repeating rainbow color scale with increasing brightness from low to high values. Lavender corresponds to means of 4.5 and above and black corresponds to means of zero. (B) The standard deviation corresponding to the same 10-s steady-state period is plotted as a function of the same stimulus parameters as in A. Standard deviations are plotted on a rainbow color scale with red corresponding to values of 6 and above and black corresponding to zero. Note that the larger standard deviations occur with lower stimulus amplitude for a range of ω from 0.70 to 0.80 ms^{-1} . (Inset) A high resolution map of standard deviations for amplitudes below $2 \mu\text{A}/\text{cm}^2$. The inset boundaries are 28–80 ms^{-1} and 1.504–40 $\mu\text{A}/\text{cm}^2$ for horizontal and vertical axes, respectively. Standard deviations greater than 0.6 are mapped in red. The inset is plotted with the same color spectrum on a scale of 0–0.6.

values ranging from 0.28 to 0.40 and this region extended even further for lower stimulus amplitudes (not shown). Together, these aperiodic regimes span a broad range of stimulus frequencies (i.e. 33–135 Hz or ω values of 0.21–0.80 ms^{-1}). The standard deviations within both aperiodic regimes fell predominantly between 0.5 and 6.0.

Aperiodic spiking patterns were very similar to the aperiodic patterns described for somatosensory fiber entrainment to near-threshold sinusoid somatic stimulation.⁴⁵ Two examples from the low-amplitude, low-frequency aperiodic regime (Fig. 2B, inset and arrow) are given, as these resemble the physiological entrainment aperiodicities.⁴⁵

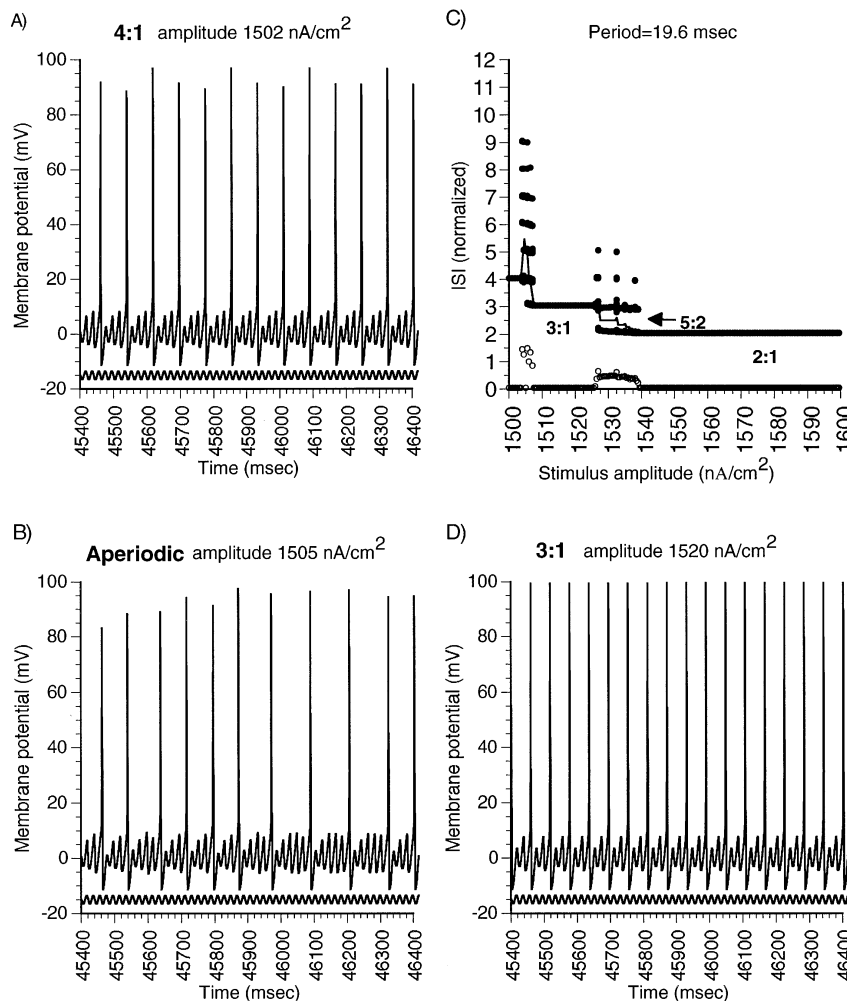


Fig. 3. Entrainment patterns vary systematically with changes in sinusoid amplitude for a fixed period of 19.6 ms ($\omega = 0.32 \text{ ms}^{-1}$). (A, B, D) Plots of membrane and stimulus potentials during a 1-s steady-state period. Entrainment patterns of 4:1, aperiodic and 2:1 are elicited with stimulus amplitudes of 1502, 1505 and 1520 nA/cm² as illustrated in A, B and D, respectively. (C) Normalized ISIs (solid circles), the mean nISI (solid line) and the standard deviation (open circles) for the 10-s steady-state period are plotted for a range of stimulus amplitudes (1500–1600 nA/cm²). Amplitude is incremented in steps of 0.5 nA/cm². Note that the regions of 2:1, 3:1 and 4:1 phase-locking are predominant. The smaller region of aperiodic entrainment is interleaved between the 4:1 and 3:1 regions. The aperiodic train is associated with a mean nISI of 5.5 and a standard deviation of 1.5.

Similar variability and additive properties were observed for aperiodic patterns in the high-frequency aperiodic regime (not shown). In the first example, the aperiodic entrainment pattern was located between regions of 4:1 and 3:1 phase-locking for a stimulus period of 19.63 ms ($\omega = 0.33 \text{ ms}^{-1}$; Fig. 3B, C). When the stimulus amplitude was increased by only 0.33% (from 1504.0 to 1504.5 nA/cm²), there was an associated increase in nISI mean (from 4 to 5.4) and standard deviation (from 0 to 1.5). The rise in standard deviation reflected the instability in spiking pattern. These patterns were considered “aperiodic” because no repeating sequence of ISIs was observed within the 10-s steady-state period (Fig. 5A, D). In the first example, spiking occurred at intervals ranging from

four to 12 times the stimulus period. In the second example, the aperiodic pattern was located between stable phase-locking patterns of 11:1 and 8:1. In this case the stimulus period and amplitude were 20.94 ($\omega = 0.34 \text{ ms}^{-1}$) and 1540 nA/cm², respectively. Normalized ISIs in the second example ranged from eight to 16 times the stimulus period. A 1-s epoch of membrane voltage is plotted for each example of aperiodic entrainment to illustrate the membrane potential variability underlying the ISI variability (Figs 3B, 4B).

For aperiodic entrainment patterns, the entire sequence of ISIs within the 10-s steady-state epoch was not predictable; however, there were patterns in the sequential order of nISIs. The distribution of repeating or “near-repeating” short ISI sequences was

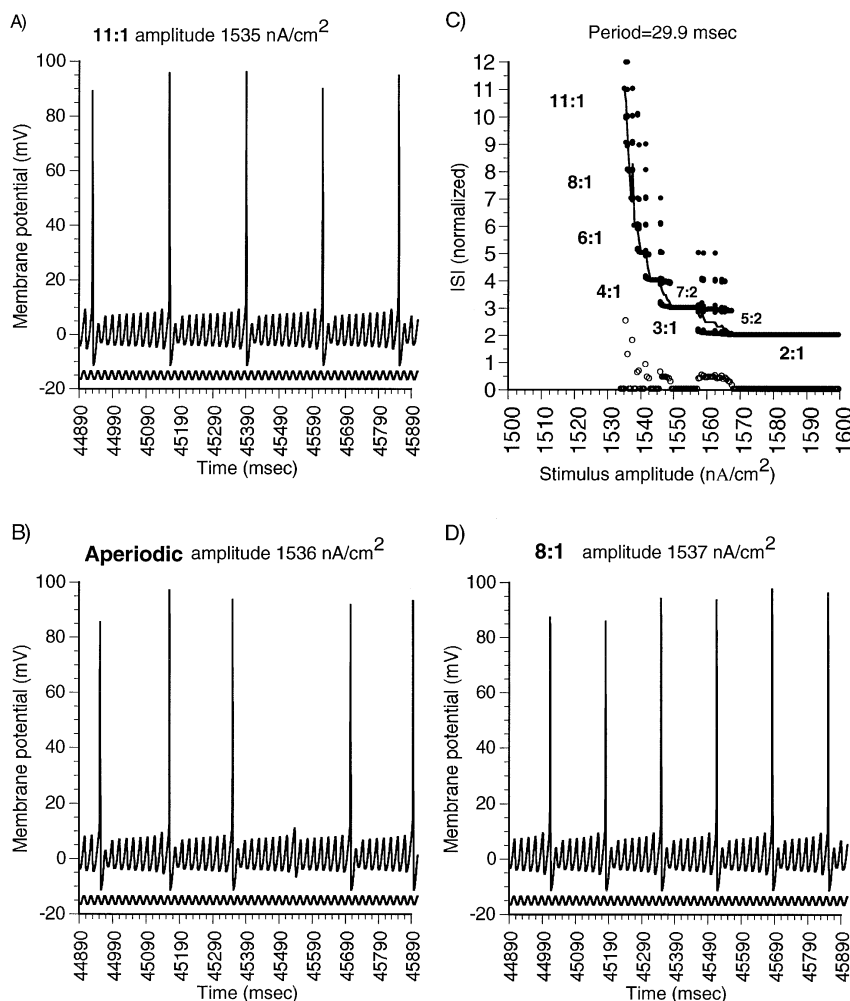


Fig. 4. Entrainment patterns vary systematically with changes in sinusoid amplitude for a fixed period of 20.9 ms ($\omega = 0.30 \text{ ms}^{-1}$). (A, B, D) Plots of membrane and stimulus potentials during a 1-s steady-state period. Entrainment patterns of 11:1, aperiodic and 8:1 are elicited with stimulus amplitudes of 1535, 1536 and 1537 nA/cm^2 as illustrated in A, B and D, respectively. (C) Normalized ISIs (solid circles), the mean nISI (solid line) and the standard deviation (open circles) for the 10-s steady-state period are plotted for a large range of stimulus amplitudes (1500–1600 nA/cm^2). Amplitude is incremented in steps of 0.5 nA/cm^2 . Note that the regions of 2:1, 3:1 and 4:1 phase-locking are predominant. One region of aperiodic entrainment is interleaved between the 11:1 and 8:1 phase-locked regions. The aperiodic train illustrated in C is associated with a mean nISI of 10.6 and a standard deviation of 2.0. Several other aperiodic sequences are generated with a stimulus period of 20.9 ms and these are associated with standard deviations greater than or equal to one, as shown in C.

examined by plotting each ISI against the ISI that followed in an ISI return map [ISI(i) versus ISI($i + 1$)]. Return maps revealed “near-repeating” nISI sequences (Fig. 5B, E). In the first example, there were extended sequences of nISIs near 4. Consequently, nISIs were heavily distributed about the point (4,4) on the return map (Fig. 5B). In contrast, there was never an incident where two or more nISIs of 5 occurred sequentially over the last 10 s of a 50-s simulation (Fig. 5B).

There were marked asymmetries in the densities and distributions of ISIs within an aperiodic sequence such that the most frequently observed ISIs were near those observed in stable entrainment patterns of neighboring regions of the parameter space.

Asymmetries in the distribution densities of ISIs were readily visualized with density histogram plots (Fig. 5C, F). When stimulus amplitude and period were 1504.5 nA and 19.63 ms, respectively, ISIs tended to be distributed about a limited set of near-integer multiples of the stimulus period (e.g., 4, 5, 6, 12). In the first example, nISIs ranged from 4 to 12, with 4, 5 and 6 being the most frequent (largest peaks in the density histogram). A small decrease in stimulus amplitude was sufficient to generate a stable pattern of 4:1 or 5:1 (e.g., 4:1, Fig. 3A). Thus, the most frequently observed ISIs in aperiodic patterns tended to be of similar normalized duration to those observed in the surrounding regions of parameter space. In the second example, nISIs were most frequently

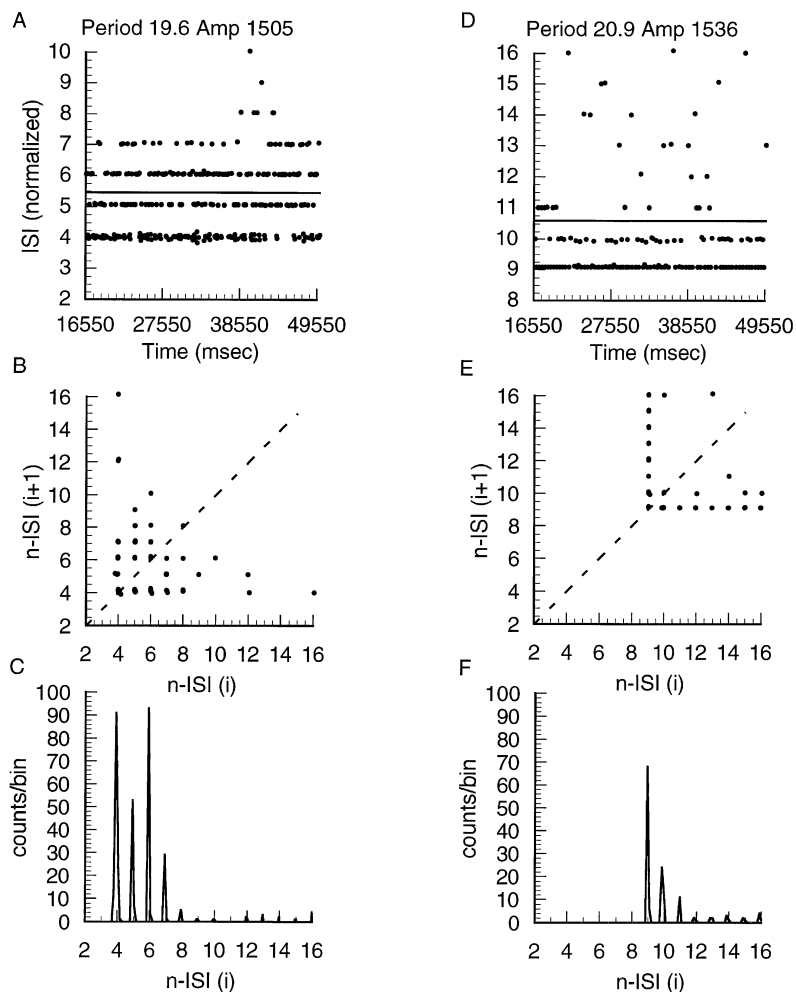


Fig. 5. Comparison between two different aperiodic sequences. (A) The time-course plot of nISIs over 33 s for a stimulus period of 19.6 ms and amplitude of 1505 nA/cm². The mean nISI (solid line) is determined from the last 10 s of the 50-s simulation. Return maps (B) and density histograms (C) for the last 10 s of the 50-s simulation are also shown. D–F are the same as A–C with a stimulus period of 20.9 ms and amplitude of 1536 nA/cm². Note the lack of overlap for the two nISI sequences.

distributed about 9, 10 and 11 (Fig. 5F, right). Similarly, a stable pattern of 11:1 was observed in neighboring regions of the parameter space (Fig. 4A). In summary, even though ISI sequences were unpredictable for a given aperiodic entrainment pattern, the range and density of ISIs were constrained by the stimulus parameters used.

Entrainment patterns for a collection of neurons

What happens to the dynamics of a sinusoidally driven neuron if it is embedded within a matrix of synaptically coupled neurons? A network of 25 coupled neurons was constructed to explore this problem. Neurons were modeled with the HH equations as above. Each neuron received synaptic input from five to 10 of its nearest neighboring neurons via a rapid depolarizing PSC (see Experimental Procedures). The model PSC followed each action potential with a short delay of 3–15 ms, depending upon

the displacement between input and target neuron. A 3-ms delay between neighboring model neurons approximated experimentally observed intracortical and interhemispheric monosynaptic delays,⁴⁷ and allowed for a rich array of autonomous firing patterns (Siegel and Read, unpublished observations). These neurons lacked the multiple compartments and sites of PSC input which can create additional temporal delays. The given parameters were selected so that this small, highly interconnected network was capable of generating a sustained output after one or more of the 25 neurons was stimulated to threshold. The range and degree of synchronous or asynchronous activity of the population model did not change appreciably when the number of neurons was increased to 100; hence, the 25-neuron model was used. Once threshold was reached for the central neuron, there was a short period of time (up to 1 s) before a spiking pattern was considered stable (e.g., Fig. 6, bottom). Thus, only those ISIs occurring in the

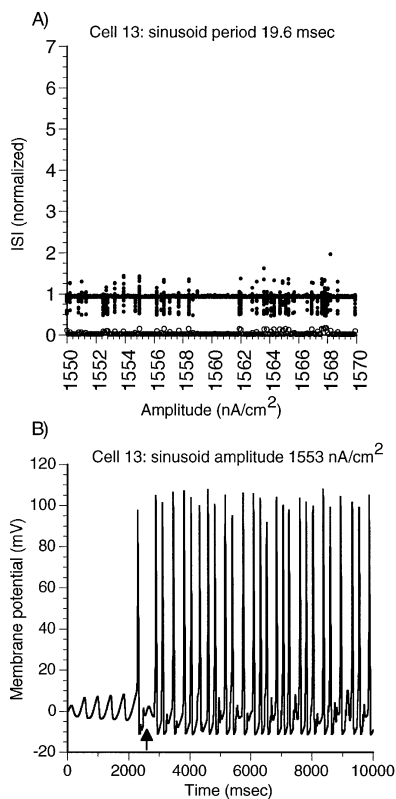


Fig. 6. Entrainment patterns for neuron 13 of the population vary with changes in sinusoid amplitude for a fixed period of 19.6 ms ($\omega = 0.32 \text{ ms}^{-1}$). (A) Normalized ISIs (nISIs; solid circles), the mean nISI (solid line beneath nISIs) and the standard deviation (open circles) for the 10-s steady-state period are plotted for a range of stimulus amplitudes (1550–1570 nA/cm^2). Aperiodic patterns are observed throughout the parameter region. (B) An example membrane potential for an aperiodic pattern is given. Note that there is no synaptic input until after neuron 13 spikes (arrow).

last 9 s of a 10-s simulation were used to assess entrainment periodicity in the population model.

Neurons embedded in the network fired either phase-locked to the sinusoid rhythm or in an aperiodic fashion, depending upon the sinusoid period and amplitude. The amplitude of the sinusoid stimulus to cell 13 was varied from 1550 to 1600 nA/cm^2 in 0.5-nA increments. Entrainment to the sinusoid rhythm was dependent upon the stimulus amplitude and frequency (e.g., Fig. 6, top). When the embedded neuron was periodically entrained to the driving stimulus, nISIs were equal to the nISI mean and the standard deviation was zero. When the neuron failed to periodically entrain, nISIs were scattered over a range of values and were associated with an increased standard deviation (Fig. 6, open circles). Sinusoid amplitudes and frequencies which resulted in phase-locked patterns for cell 13 also entrained the entire population to a common rhythm. Similarly, those stimulus conditions that generated aperiodic output in the driven neuron resulted in an asynchronous mode of output from the population. For example,

the aperiodic activity of neuron 13 in Fig. 6 (bottom) was associated with asynchronous output from the coupled population (not shown). Hence, the entrainment pattern of a single neuron (cell 13) reflected the entrainment activity of the entire population.

Embedding the sinusoid driven neuron within an excitatory network dramatically restricted the range of entrainment patterns. Higher order phase-locked patterns (e.g., low-frequency entrainment such as 11:1, 5:1, 3:1) were no longer observed in the population model. The most prominent phase-locked pattern in the population-coupled neuron was a pattern of 1:1 phase-locking with nISIs near a mean of 1. When neuron 13 was driven with a sinusoid period of 19.6 ms, aperiodic ISI sequences were common. The ISIs within an aperiodic sequence were restricted to a range of 3.92–39.2 ms or an nISI range of 0.2–2 (sinusoid period = 19.6 ms; Fig. 6, top). It is noteworthy that this is a biologically feasible range of entrainment frequencies, as ISIs of 39.2–3.92 ms correspond to frequencies of 25–255 Hz. The short ISIs associated with periodic and aperiodic entrainment in the population were a reflection of the short delay in feedback from neighboring neurons.

DISCUSSION

Sinusoidal stimulated HH differential equations were used to model the basic features of entrainment of an isolated neuron and a neuron embedded within a population of synaptically coupled neurons. The resting state of the HH neuron was quiescent, i.e., there was no baseline spiking prior to sinusoid current input. ISIs were normalized to the stimulus period, and means and standard deviations of nISIs were used as measures of entrainment. Spiking of HH neurons was phase-locked for most stimulus conditions. Systematic variation of the stimulus amplitude and period revealed ordered transitions between mean ISIs and phase-locked patterns, the order of which was predictable according to a simple additive rule (Farey summation). Higher order and aperiodic entrainment patterns were observed interleaved between the more stable phase-locking domains of the parameter space (Fig. 2B). Thus, the hypothesis that aperiodic entrainment patterns arise in part from the membrane conductance dynamics was supported. However, aperiodic patterns of entrainment were more prevalent when there was feedback from a population affecting the periodically driven neuron.

Farey trees

Farey summation between neighboring phase-locking domains within the frequency–amplitude parameter space is a general property of both “threshold” and “coupled” oscillatory systems.^{1,3,16,27} Threshold oscillatory systems are those systems that have a threshold for generating oscillatory output.^{2,27} Many nerve fibers or neurons are

quiescent in the resting state and can be considered to have a threshold for oscillatory (spike) output.^{4,11,33,40,45} Systems that oscillate intrinsically at rest are considered as coupled oscillatory systems when driven with an extrinsic rhythmic input. A resting or baseline oscillatory state is the natural state of cardiac fibers¹⁶ and it is induced experimentally in neurons by lowering the external calcium concentrations^{1,27} or by injecting depolarizing bias current.^{8,19,21} In both systems the phase-locked entrainment patterns vary systematically with changes in stimulus amplitude and frequency,^{1,17,19,21,27,31,32} and these entrainment patterns can be predicted with the simple Farey summation rule^{12,15,39} (Results and Fig. 2).

The frequency–amplitude parameter space of the threshold system is sufficiently different from that of coupled oscillatory systems so that the parameter space effectively serves as a “fingerprint” of the system. In threshold systems, such as the quiescent HH neuron, input currents of low frequency and low amplitude fail to evoke sodium spikes or resulting ISIs (Fig. 2A). As either frequency or amplitude is systematically increased there is a monotonic increase in firing rate. Neighboring regions of different entrainment patterns originate and diverge from a common (or critical) point in the frequency–amplitude parameter space. Neighboring regions with different entrainment patterns abut one another so that changes in entrainment pattern with stimulus parameters are abrupt. Conversely, when an HH neuron (or cardiac fiber) is placed into a state of rhythmic activity prior to entrainment, the boundaries of entrainment regions are less discrete. A systematic increase in frequency and amplitude does not lead to a monotonic increase in firing rate. In coupled oscillatory systems, the different entrainment regions no longer arise from a common point; they arise instead from separate points to form “tongue”-like structures.^{1,15,17,32} Transitions from one entrainment region to the next are less abrupt. This separation of entrainment regimes is a hallmark difference between the two types of systems. We refer to the convergence of the threshold parameter space into tightly packed phase-locking regions as a “folding” of the parameter space and, conversely, to the separation of these regimes in the coupled oscillatory system as an “unfolding”.

Aperiodic regimes

Aperiodic entrainment regimes have been well documented for entrainment of coupled oscillatory systems,^{17,19,21,32,38,39} however, they are less well documented for the threshold systems. Aperiodic entrainment regimes were observed in the folded parameter space of the HH neuron with a threshold for output (Figs 2–4), thereby confirming predictions from (i) experimental systems and (ii) a simple mathematical model. Systematic transitions from periodic

to aperiodic firing have been demonstrated for neurons that fire infrequently or not at all prior to stimulus input.^{19,21,31,45} Furthermore, the genesis of aperiodic patterns from the HH differential equations (with a threshold) had been predicted from a linearized model, the Fitzhugh–Nagumo equations.² That the higher order phase-locking and interleaved aperiodic regimes were conserved in the more realistic HH model suggests that the origin of aperiodicities from the system is a robust phenomenon (i.e. these regions were not obscured by small integration errors). The exact temporal sequence for aperiodic output, given a set of parameters, was not predictable. However, the frequency distribution of ISIs for aperiodic regimes overlapped with those of neighboring phase-locked regions of frequency–amplitude parameter space (e.g., Figs 3, 4). Hence, the mean frequency of spiking in aperiodic regimes was somewhat predictable. Larger aperiodic regimes were observed on the borders between phase-locking domains with HH equations (and simpler models) that have been adjusted to allow for sustained oscillation prior to periodic stimulation.^{17,19,21,32,38,39} It had been suggested that the presence of a “carrier” frequency or baseline oscillatory state increased these regions of aperiodicity, though a mechanism was not offered.²¹ Since aperiodic patterns in either system tended to occur on the borders of phase-locking domains, it is possible that the increase in aperiodic domains stemmed from the unfolding of the frequency–amplitude parameter space observed in coupled oscillatory systems.

If the presence of an intrinsic “carrier” frequency or baseline output of a single neuron has the effect of unmasking new aperiodic entrainment patterns, then what effect does feedback from a population of neurons have? Unlike the primary somatosensory fibers, most secondary sensory or central neurons are synaptically coupled to a matrix of neurons. In the present model, a single neuron was driven by sinusoid input to emulate a periodic afferent drive (or sensory stimulus). Embedding the sinusoidally driven neuron within a population of neurons dramatically altered the model neuron’s entrainment properties and increased the incidence of aperiodic entrainment. High-order, low-frequency phase-locking was eliminated and regions of aperiodicity were expanded in the frequency–amplitude parameter space (compare Fig. 1 and Fig. 6). Furthermore, the output during aperiodic or periodic entrainment was restricted to a frequency range of 25–255 Hz. Thus, in this simplified population model aperiodic entrainment was a dominant pattern and spiking fell within a narrow band of frequencies.

Physiological implications

Aperiodic or “noisy” entrainment to a periodic stimulus is a common feature of *in vivo* neural ensembles; however, the source and nature of such aperiodicities have not been determined. Rhythmic

synaptic drive or membrane potential oscillations are ubiquitous phenomena in nervous systems,^{2,6,9,14,25,45} and yet neuronal spike train output is generally not periodic itself, i.e., entrainment is aperiodic. In the somatosensory system, aperiodic entrainment is observed in primary sensory fibers and is even more prevalent in second order sensory neurons.^{29,45} A subpopulation of hippocampal and entorhinal neurons fires in phase with a 200-Hz afferent drive (ripple).⁶ The output of hippocampal neurons is correlated but aperiodic or intermittent with respect to the 200-Hz afferent drive. Clearly, one source of aperiodicity in such neuronal populations is the random membrane fluctuations caused by synaptic or membrane channel “noise”^{7,26,42} (cf. Liebovitch²⁴). Accordingly, spontaneous ISI or synaptic potential data from some sensory and motor neurons can be approximated by Poisson or Gaussian distributions,^{13,35,37} and the data distribution can be approximated in simulations by adding a stochastic element to account for random membrane fluctuations.^{7,19,26,41,42,44} However, simply driving a model or real neuron with a random input is not a sufficient way to generate highly variable spike trains under all stimulus conditions (e.g., low-amplitude random current fluctuations^{35,44}). Indeed, evidence to the contrary exists^{21,44,46} and suggests that either (i) Poisson fits of experimental spike data have to be questioned⁴⁶ or (ii) existing models for simulating such distributions have to be modified. A second source of “jitter” for entrainment of sensory neurons could be non-stochastic properties such as those modeled here, including (i) inherent membrane properties, (ii) synaptic potential kinetics and (iii) axonal conductance delays.^{13,17,45} It will be of great interest in future studies to (i) identify unique frequency ranges of biological jitter and (ii) determine the role, if any, such jitter has in information processing in the brain.

In the past, biologists have studied physiological mechanisms for improving signal-to-noise ratios with the tacit assumption that we, as observers, know the difference between signal and noise in the brain.³⁵ The change in mean firing rate that occurs immediately following sensory stimulation is generally considered a meaningful signal in sensory neurons at all

levels, including cortical. Hence, manipulations which decrease “baseline” firing rates and increase stimulus-specific firing rates are categorized as signal enhancing.²⁸ Unfortunately, stimulus-specific changes in mean firing are operationally defined and other sensory event- and neural network-related spiking patterns may go undetected when mean firing rate is the sole measure of signal.³⁵ Accordingly, Vaadia *et al.*⁴⁸ found behavior-related changes in temporal patterns which were not associated with changes in mean firing rate and Nakamura,³⁰ Optican³⁴ and their respective colleagues found stimulus-specific temporal spike or burst patterns. Thus, distinct stimuli for sensory neuron activation may be associated with the emergence of unique temporal patterns of output. Spike train patterns need not be transmitted spike for spike in order for temporal patterns to be meaningful to target neurons. Indeed, higher order spiking patterns generated when a neuron (or population of neurons) fails to spike on every stimulus cycle (e.g., 3:2 or aperiodic) may more effectively activate, or conceivably potentiate, recipient neurons.^{22,23,35}

CONCLUSIONS

We have shown that there are differences in the patterns of activity that may evolve from individual neurons and populations of interconnected neurons. The single neuron tends to follow the stimulus in a periodic phase-locked pattern, whereas the population tends to fire aperiodically over a large stimulus regime. Such irregular dynamics are often found *in vivo* in neurons that are part of highly interconnected neural networks. However, it remains an open question whether these complicated dynamics recorded in the brain arise in part from deterministic interactive mechanisms, as posited here, or solely from the presence of stochastic processes.

Acknowledgements—We extend our thanks to Dr Charles Tresser for discussions of oscillatory system dynamics, and to Drs Leon Glass and James Chrobak for comments on the manuscript. This work was supported by NIH R01 EY09223, ONR N00014-92-1-0334 and a Henry Rutgers Fellowship.

REFERENCES

1. Aihara K. (1984) Periodic and non-periodic responses of a periodically forced Hodgkin–Huxley oscillator. *J. theor. Biol.* **109**, 249–269.
2. Alexander J. C., Doedel E. J. and Othmer H. G. (1990) On the resonance structure in a forced excitable system. *SIAM J. appl. Math.* **50**, 1373–1418.
3. Alonso A. and Klink R. (1993) Differential electroresponsiveness of stellate and pyramidal-like cells of medial entorhinal cortex layer II. *J. Neurophysiol.* **70**, 128–143.
4. Bishop P. O. (1984) Processing of visual information within the retinostriate system. In *The Handbook of Physiology: The Nervous System III* (Section 1) (ed. Darian-Smith I.), pp. 341–424. Waverly Press, Baltimore.
5. Brown T. H. and Johnston D. (1983) Voltage-clamp analysis of mossy fiber synaptic input to hippocampal neurons. *J. Neurophysiol.* **50**, 487–507.
6. Buszák G., Bragin A., Chrobak J. J., Nadasdy Z., Sik A. and Hsu M. and Ylinen A. (1994) Oscillatory and intermittent synchrony in the hippocampus: relevance to memory trace formation. In *Temporal Coding in the Brain* (eds Buszák G., Llinás R., Singer W., Berthoz A. and Christen Y.), pp. 145–169. Springer, Berlin.
7. Calvin W. H. and Stevens C. F. (1968) Synaptic noise and other sources of randomness in motoneuron interspike intervals. *J. Neurophysiol.* **31**, 547–587.

8. Canavier C. C., Clark J. W. and Byrne J. H. (1990) Routes to chaos in a model of a bursting neuron. *Biophys. J.* **57**, 1245–1251.
9. Carr C. E., Heiligenberg W. and Rose G. J. (1986) A time-comparison circuit in the electric fish midbrain. I. Behavior and physiology. *J. comp. Neurol.* **314**, 306–318.
10. Coon D. D., Ma S. N. and Perera G. U. (1987) Farey-fraction frequency modulation in the neuron-like output of silicon $p-i-n$ diodes at 4.2 K. *Phys. Rev. Lett.* **58**, 1139–1142.
11. Darian-Smith I. (1984) Thermal sensibility. In *The Handbook of Physiology: The Nervous System III* (Section 2) (ed. Darian-Smith I.), pp. 341–424. Waverly Press, Baltimore.
12. Feigenbaum M. (1988) Complicated objects on regular trees. In *Nonlinear Evolution and Chaotic Phenomena* (eds Gallavotti G. and Zweifel P.), pp. 10–21. Plenum Press, New York.
13. Freeman W. J. (1975) *Mass Action in the Nervous System*. Academic Press, New York.
14. Fregnac Y. and Bringuier V. and Baranyi A. (1994) Oscillatory neuronal activity in visual cortex: a critical re-evaluation. In *Temporal Coding in the Brain* (eds Buzáki G., Llinás R., Singer W., Berthoz A. and Christen Y.), pp. 81–102. Springer, Berlin.
15. Glass L. and Mackey M. C. (1988) Periodic stimulation of biological oscillators. In *From Clocks to Chaos. The Rhythms of Life*. Princeton University Press, Princeton, NJ.
16. Glass L., Guevara M. R. and Shrier A. (1987) Universal bifurcations and the classification of cardiac arrhythmias. *Ann. N. Y. Acad. Sci.* **504**, 168–178.
17. Guevara M. R., Glass L., Mackey M. C. and Shrier A. (1983) Chaos in neurobiology. *IEEE Trans. Syst. Mangmt. Cybern.* **5**, 790–798.
18. Guevara M. R., Glass L. and Shrier A. (1981) Phase-locking, period-doubling bifurcations, and irregular dynamics in periodically stimulated cardiac cells. *Science* **214**, 1350–1353.
19. Guttman R., Feldman L. and Jakobsson E. (1980) Frequency entrainment of squid axon membrane. *J. Membrane Biol.* **56**, 9–18.
20. Hodgkin A. L. and Huxley A. F. (1952) A quantitative description of membrane current and its application to conduction and excitation in nerve. *J. Physiol.* **117**, 500–544.
21. Holden A. V. (1976) The response of excitable membrane models to a cyclic input. *J. Cybern.* **21**, 1–7.
- 21a. Jack J. J. B. and Noble D. and Tsien R. W. (1975) *Electric Current Flow in Excitable Cells*. Oxford University Press, London.
22. Klemm W. R. and Sherry C. J. (1982) Do neurons process information by relative intervals in spike trains?. *Neurosci. Biobehav. Rev.* **6**, 429–437.
23. Larson J. and Lynch G. (1986) Induction of synaptic potentiation in hippocampus by patterned stimulation involves two events. *Science* **232**, 985–988.
24. Liebovitch L. S. (1993) Interpretation of protein structure and dynamics from the statistics of the open and closed times measured in a single ion-channel protein. *J. stat. Phys.* **70**, 329–337.
25. Llinás R. R., Grace A. A. and Yarom Y. (1991) *In vitro* neurons in mammalian cortical layer 4 exhibit intrinsic oscillatory activity in the 10- to 50-Hz frequency range. *Proc. natn. Acad. Sci. U.S.A.* **88**, 897–901.
26. Longtin A. (1993) Stochastic resonance in neuron models. *J. stat. Phys.* **70**, 309–327.
27. Matsumoto G., Aihara K., Hanyu Y., Takahashi N., Yoshizawa S. and Nagumo J. (1987) Chaos and phase locking in normal squid axons. *Physics* **A123**, 162–165.
28. McCormick D. A. (1989) Cholinergic and noradrenergic modulation of thalamocortical processing. *Trends Neurosci.* **12**, 215–221.
29. Mountcastle V. B., Steinmetz M. A. and Romo R. (1990) Frequency discrimination in the sense of flutter: psychophysical measurements correlated with postcentral events in behaving monkeys. *J. Neurosci.* **10**, 3032–3044.
30. Nakamura K., Mikami A. and Kubota K. (1991) Unique oscillatory activity related to visual processing in the temporal pole of monkeys. *Neurosci. Res.* **12**, 293–299.
31. Nemoto I., Miyazaki S., Saito M. and Utsunomiya T. (1975) Behavior of solutions of the Hodgkin–Huxley equations and its relation to properties of mechanoreceptors. *Biophys. J.* **15**, 469–479.
32. Nomura T., Sato S., Doi S., Segundo J. P. and Stiber M. D. (1993) A Bonhoeffer–van Pol oscillator model of locked and non-locked behaviors of living pacemaker neurons. *Biol. Cybern.* **69**, 429–437.
33. Norgren R. (1984) Central neural mechanisms of taste. In *The Handbook of Physiology: The Nervous System III* (Section 2) (ed. Darian-Smith I.), pp. 341–424. Waverly Press, Baltimore.
34. Optican L. M. and Richmond B. J. (1987) Temporal encoding of two-dimensional patterns by single units in primate inferior temporal cortex. *J. Neurophysiol.* **57**, 167–178.
35. Perkel D. H. and Bullock T. H. (1968) Neuronal coding: a report based on an NRP work session. *Neurosci. Res. Program Bull.* **6**, 221–348.
36. Press W. H., Flannery B. P. and Teukolsky S. A. and Vetterling W. T. (1988) Integration of ordinary differential equations. In *Numerical Recipes*, pp. 547–577. Cambridge University Press, Cambridge.
37. Prucnal P. R. and Teich M. C. (1983) Refractory effects in neural counting processes with exponentially decaying rates. *IEEE Trans. Syst. Mangmt. Cybern.* **13**, 1023–1033.
38. Rinzel J. and Miller R. N. (1980) Numerical calculation of stable and unstable periodic solutions to the Hodgkin–Huxley equations. *Math. Biosci.* **49**, 27–59.
39. Sato S. and Doi S. (1992) Response characteristics of the BVP neuron model to periodic pulse inputs. *Math. Biosci.* **112**, 243–259.
40. Scheibel A. B. (1984) The brain stem reticular core and sensory function. In *The Handbook of Physiology: The Nervous System III* (Section 1) (ed. Darian-Smith I.), pp. 213–256. Waverly Press, Baltimore.
41. Siegel R. M. (1990) Non-linear dynamical system theory and primary visual cortical processing. *Physica D* **42**, 385–395.
42. Siegel R. M. and Read H. L. (1993) Models of the temporal dynamics of visual processing. *J. stat. Phys.* **70**, 297–308.
43. Siegel R. M., Tresser C. and Zettler G. (1992) A decoding problem in dynamics and in number theory. *Chaos* **2**, 473–494.
44. Stein R. B. (1967) Some models of neuronal variability. *Biophys. J.* **7**, 37–68.

45. Talbot W. H., Darian-Smith I., Kornhuber H. H. and Mountcastle V. B. (1968) The sense of flutter-vibration: comparison of human capacity with response patterns of mechanoreceptive afferents from the monkey's hand. *J. Neurophysiol.* **31**, 302-334.
46. Teich M. C. and Khanna S. M. (1985) Pulse-number distribution for the neuronal spike train in the cat's auditory nerve. *J. acoust. Soc. Am.* **77**, 1110-1128.
47. Thomson A. M. (1986) A magnesium-sensitive post-synaptic potential in rat cerebral cortex resembles neuronal responses to *N*-methylaspartate. *J. Physiol.* **370**, 531-549.
48. Vaadia E., Haalman I., Abeles M., Bergman H., Prut Y., Slovin H. and Aertsen A. (1995) Dynamics of neuronal interactions in monkey cortex in relation to behavioral events. *Nature* **373**, 515-518.

(Accepted 26 March 1996)